Available online at www.sciencedirect.com
SCIENCE DIRECT®

Journal of the European Ceramic Society 23 (2003) 1751–1759

www.elsevier.com/locate/jeurceramsoc

Effect of lattice defects on the thermal conductivity of β-Si_3N_4

H. Yokota*, H. Abe, M. Ibukiyama

Research Center, Denki Kagaku Kogyo K.K 3-5-1, Asahi-cho, Machida-city 194-8560 Tokyo, Japan

Received 1 March 2002; received in revised form 25 September 2002; accepted 5 October 2002

Abstract

Two types of β-Si_3N_4 were sintered at 1900 °C one for 8 h and the other for 36 h by using Yb_2O_3 and ZrO_2 as sintering additives. The latter specimen was further annealed at 1700 °C for 100 h to promote grain growth. The microstructures of the sintered materials were investigated by SEM, TEM, and EDS. The thermal conductivities of the specimens were 110 and 150 $Wm^{-1}K^{-1}$, respectively. The sintered material which possessed 110 $Wm^{-1}K^{-1}$ had numerous small precipitates that consisted of Yb, O and N elements and internal dislocations in the β-Si_3N_4 grains. In the sintered material with 150 $Wm^{-1}K^{-1}$ neither precipitates nor dislocations were observed in the grains. The microscopic evidence indicates that the improvement in the thermal conductivity of the β-Si_3N_4 was attributable to the reduction of internal defects of the β-Si_3N_4 grains with sintering and annealing time as the grains grew.

Keywords: Defects; Grain growth; Grain size; Impurities; Si_3N_4; TEM; Thermal conductivity

1. Introduction

The conduction of heat in ceramics is dominated by phonon transport. It is well-known that phonon scattering is attributed to imperfections in the crystal lattice such as impurities, vacancies, interstitials and dislocations at room temperature. [1] Recently, a significant increase in thermal conductivity of sintered β-Si_3N_4, i.e. over 100 $Wm^{-1}K^{-1}$, has been achieved by using high-purity raw powders with effective sintering additives.[2–7] Recent investigations on thermal conductivities of β-Si_3N_4 ceramics revealed that lattice oxygen content is a crucial factor governing the thermal conductivity of this material. [8–10] In a previous work, we[11,12] reported that a precise chemical analysis of sintered β-Si_3N_4 grains was performed, and as a result, the major impurity in the β-Si_3N_4 crystal lattice was oxygen, but the contents of the impurities except aluminum in the β-Si_3N_4 lattice decreased with grain growth. Hence, the key technology for obtaining high thermal conductivity is to realize the "purification-promoted grain growth" with effective additives, except aluminum contained oxides or nitrides.

The imperfections in the crystal lattice, other than oxygen impurities as mentioned above, also affect thermal conductivity of materials. There have been several reports concerning defects in the β-Si_3N_4 grains.[13–16] However, there have been few studies concerning the relation between thermal conductivity and the internal structure of the β-Si_3N_4.[5,17] It is therefore important to investigate such relations including vacancies, interstitials and dislocations. These sintered β-Si_3N_4[5,17] ceramics were fabricated at very high sintering temperature of 2200 °C by Hiping, so that it is desirable to understand the phenomena around normal pressureless sintering from a technological standpoint.

In a previous work, [18,19] we reported that the thermal conductivities when sintered with Yb_2O_3/ZrO_2 as sintering additives were higher than those with Y_2O_3/HfO_2 and the maximum thermal conductivities of over 140 $Wm^{-1}K^{-1}$ with an isotropic microstructure were obtained by a pressureless sintering. It is realized that the composition and dihedral angle of the grain boundary phases play a significant role in the thermal conductivity of the sintered ceramics. Grain boundary film thickness,[20] grain boundary phases,[21] and amount of secondary phases[20] all affect thermal conductivity. The compositions of the grain boundary phases sintered with Y_2O_3 changed with grain growth.[12] With regard to

* Corresponding author. Fax: +81-427-21-3693.
E-mail address: hiroshi-yokota@denka.co.jp (H. Yokota).

0955-2219/03/$ - see front matter
PII: S0955-2219(02)00374-6

the Yb_2O_3 additives, the composition of the grain boundary phase did not change with grain growth,[19] so in order to investigate what really happened in β-Si_3N_4 grains with increasing thermal conductivities, it is easier to investigate for the Yb_2O_3 additives than for the Y_2O_3 additives. Further, it is easier for the Yb_2O_3 additives than for the Y_2O_3 additives to obtain higher thermal conductivities, so the choice of the Yb_2O_3 additives for understanding the relation between thermal conductivity and internal structure of the grains via purification-promoted grain growth is effective.

The objective of the present study is thus to investigate the internal structure of the β-Si_3N_4 grains with different thermal conductivities, i.e. 110 and 150 $Wm^{-1}K^{-1}$.

2. Experimental procedures

The specimens were prepared from a high purity silicon nitride raw powder and sintering aids. The specifications of raw β-Si_3N_4 powder (Grade NP-400, Denki Kagaku Kogyo, Tokyo, Japan), obtained by direct nitridation of silicon is shown in Table 1. The raw silicon nitride powder and 10 mass% Yb_2O_3 (purity >99.9%, BET 4 m^2/g, Shin-etsu Chemical, Tokyo, Japan) and 2 mass% ZrO_2 (purity >99.9%, BET 4 m^2/g, Soekawa Chemical, Tokyo, Japan) were ball milled for 3 h using methanol as the solvent. After drying, the powder mixtures were prepared for sintering. Approximately 2 g of the dried powder was uniaxially pressed under 20 MPa in a die 12.5 mm in diameter. The pellet was then isostatically cold-pressed under a pressure of 200 MPa. The CIPped pellet was placed in a BN crucible. Sample A was sintered in a graphite furnace at 1900 °C for 8 h under a nitrogen pressure of 0.9 MPa. On the other hand, sample B was sintered at 1900 °C for 36 h, subsequent heat treatment was performed at 1700 °C for 100 h to promote grain growth. The densities of the specimens were measured by the Archimedes method.

To evaluate the thermal conductivity, disks 10 mm in diameter and 3 mm in thickness were cut from the sintered materials. Thermal conductivity at room temperature was calculated from the equation.

$$K = \alpha C_p \rho \quad (1)$$

The thermal diffusivity (α) and the specific heat (C_p) of the specimens were measured at room temperature by a laser flash method using a thermal constant analyzer (TC-3000, ULVAC, Japan). The specific heat, 0.67 J/g-K, was used in this work.

Phase identification of the sintered materials was performed by X-ray diffractometry (XRD). The microstructure of the sintered materials was examined by scanning electron microscopy (SEM, JSM-820, Jeol, Tokyo, Japan) of polished and CF_4 plasma etched surfaces. Thin foils for transmission electron microscopy (TEM, JEM-2010, Jeol, Tokyo, Japan) were prepared by the standard procedures of grinding, dimpling, and argon-ion-beam thinning, followed by carbon coating to minimize charging during observation. The TEM examinations were performed in 200 kV with a Tracer EDS system for 100 adjacent grains in each specimen. The compositions of the interesting regions within the grains were analyzed by EDS. The EDS was equipped with a cold field emission electron gun. The spatial resolution available with this instrument is 3 nm. In order to measure the intergranular film thickness accurately, the specimen was tilted so as to align the grain boundary "edge-on" and also to orient adjacent grains in good diffracting conditions.[22]

Table 1
Properties of raw Si_3N_4 powder

Property	
α- Phase content/mass%	48.5
Purity	
Oxygen/mass%	0.75
Aluminum/ppm	120
Calcium/ppm	70
Iron/ppm	40
BET specific surface area/m^2g^{-1}	14.7

3. Results

The results of weight loss, densities, thermal diffusivities, and thermal conductivities of the specimens are shown in Table 2. The reason for the lower density and higher weight loss of sample B is attributed to the longer sintering time and additional annealing. Since sample B was densified to near full density at the middle stage of

Table 2
Sintering and annealing conditions, weight loss, densities, thermal diffusivities, and thermal conductivities of the specimens

	Sintering and annealing conditions	Weight loss (mass%)	Density (g/cm^3)	Thermal diffusivity (cm^2/s)	Thermal conductivity ($Wm^{-1}K^{-1}$)
Sample A	1900 °C × 8 h	2.52	3.40	0.4758	110
Sample B	1900 °C × 36 h → 1700 °C × 100 h	7.53	3.33	0.6723	150

the sintering, vaporization of substances from the specimens might have occured.[9] Thermal diffusivity and thermal conductivity of sample B were much higher than those of sample A. Thermal conductivity of sample B was 150 $Wm^{-1}K^{-1}$, which is approximately as high as the prolonged time sintered materials with Yb_2O_3–$MgSiN_2$ additives.[9]

Fig. 1 shows relatively low magnification SEM photographs of sample A and B. Both specimens had a bimodal and randomly oriented microstructure composed of small matrix grains and large elongated grains. It was clear that sample B contained a larger amount of the large elongated β-Si_3N_4 grains than sample A. Thus, the longer sintering time in comparison with sample A, and the additional heat treatment of sample B significantly promoted grain growth of β-Si_3N_4.

Fig. 2 shows a bright field TEM image of the general microstructure of sample A. It was observed that there were numerous small precipitates (marked by black arrows) in the β-Si_3N_4 grains. No precipitates in the β-Si_3N_4 grains with $\geqslant 2$ μm in a diameter were observed. Scrutinizing across the grains with <2 μm in a diameter reveals the presence of precipitates is independent of the grain size. The precipitates were not observed at grain boundaries.

More detailed bright field TEM examination of the β-Si_3N_4 grains with the precipitates shows that there are obvious mismatch dislocations (marked by black arrows) across the precipitates (Fig. 3a). The mismatch dislocation would seem to exist between inside of the grain and the grain boundary. Some of the precipitates were observed without the mismatch dislocations.

Fig. 3b is a detailed bright field TEM photograph. It shows that about 50% of the β-Si_3N_4 grains of the specimen with 110 $Wm^{-1}K^{-1}$ contain some defects such as precipitates, mismatch dislocations (marked by white arrows), and the dislocations without precipitates (marked by black arrows). The dislocations without precipitates seem to be similar to "grown in" [13] dislocations. In contrast, mismatch dislocations with precipitates were probably the result of strain fields due to the presence of precipitates. The difference between mismatch dislocations and grown in dislocations is that the latter do not contain precipitates and terminate inside of β-Si_3N_4 grains.

Fig. 4 shows an enlargement of the bright field TEM micrograph inside of a β-Si_3N_4 grain which contains many precipitates. The shape of the precipitates is either hexagonal or spherical with diameters between 10 and 30 nm. The diameters of the round particles are smaller than those of the hexagonal ones. With regard to the hexagonal particles, amorphous patterns and circular microcrystallines having a lattice image were observed in the photograph. On the other hand, the round particles were observed as crystallines. These indicate that the precipitates had a microstructure composed of small microcrystalline and amorphous phases.

Fig. 5a shows an EDS spectrum obtained from a round precipitate (marked by "a" in Fig. 4), revealing that clear peaks of Yb, O and N and weak peaks of Ca and Fe were detected. The presence of Si element could

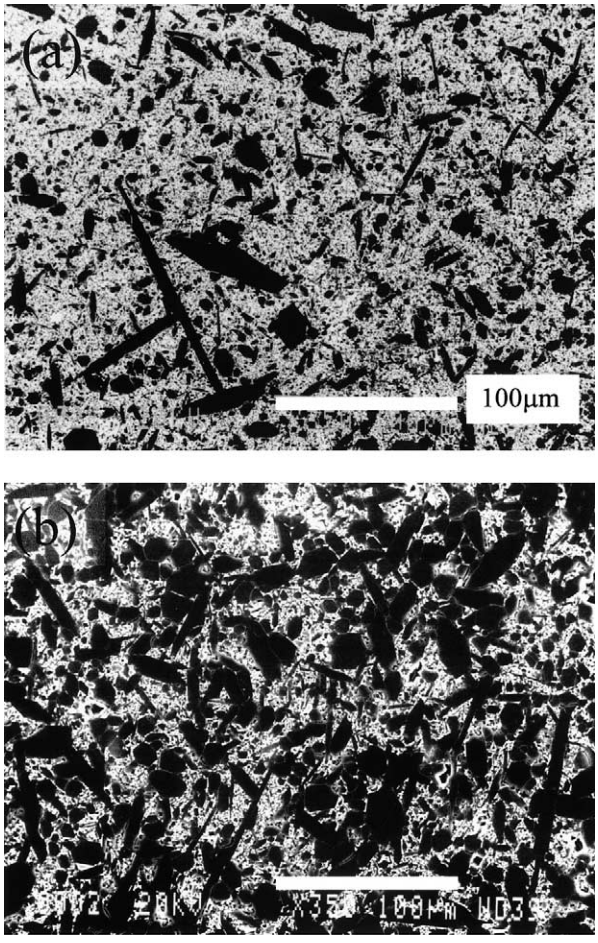

Fig. 1. SEM photographs of (a) sample A sintered at 1900 °C for 8 h and (b) sample B sintered at 1900 °C for 36 h and subsequent annealed at 1700 °C for 100 h.

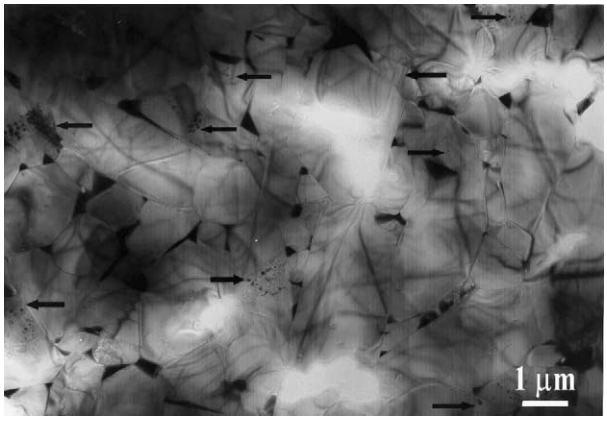

Fig. 2. Bright-field (BF) TEM image of the general microstructure of sample A.

not be confirmed due to the overlap of the Yb peak at 1.8 keV in the EDS spectrum. Fig. 5b shows an EDS spectrum obtained from a hexagonal precipitate (marked by "b" in Fig. 4), revealing that the precipitate contains the same elements as observed in the round precipitate but the hexagonal precipitate contains fewer Ca and Fe impurities. The XRD analysis shows that the $Yb_4Si_2O_7N_2$ (J) phase and the $Zr_4Yb_4O_{12}$ phase were identified. The sintered materials of this study were densified by using Yb_2O_3 and ZrO_2 as sintering additives, so Yb-Si–O–N and Zr–Yb–O liquid phase were formed during sintering. This indicates that the precipitates originate from one kind of the liquid phase.

In contrast, Fig. 5c shows an EDS spectrum from the region adjacent to the precipitates in the β-Si_3N_4 grains (marked by "c" in Fig. 4), revealing that the adjacent region contains only Si and N.

Fig. 6 shows a bright field TEM image of another region of sample A and Fig. 7a shows an EDS spectrum of the grain boundary phase marked "a" in Fig. 6. The EDS analysis indicates that Yb, O and N are present in the secondary phase within the range 1–2 μm in diameter (a small grain boundary pocket), and the chemical composition is similar to the precipitates found in Fig. 5a. Again, the presence of Si could not be confirmed due to the overlap of the Yb peak.

Fig. 7b also shows an EDS spectrum of the grain boundary phase marked "b" in Fig. 6. The EDS analysis indicates that the elements Zr, Yb, O and N are present in the secondary phase (a large grain boundary pocket) with $\geqslant 5$ μm in diameter. Fe and Ca found in the grain boundary phases probably originate from the Si_3N_4 raw powder because the raw powder contained Fe and Ca as impurities.

Fig. 8 shows a bright field TEM image of the general microstructure of the sample B. From a comparison of microstructures of these β-Si_3N_4 (see Figs. 2 and 8), it is obvious that grain size of sample B is much larger than that of sample A. Fig. 8 also shows there are no small precipitates in the β-Si_3N_4 grains and the grain boundaries. In addition, it was not observed that the β-Si_3N_4 grains of this material had dislocations without precipitates, which were observed in sample A.

For both specimens, XRD analysis identified the $Yb_4Si_2O_7N_2$ (J) phase and the $Zr_4Yb_4O_{12}$ phases. Thus, the grain-boundary phases of the specimens were independent of thermal conductivity in the present work.

The TEM micrographs in Fig. 9a and 9b depict two small regions of the grain boundaries of sample A and B shown in Figs. 2 and 8, respectively. The observed thickness of the intergranular films of the two specimens were 0.84 nm (standard deviation = 0.12 nm) and 0.82 nm (standard deviation = 0.09 nm), respectively. The intergranular film thickness data was determined at 10 locations. Since the film thickness for β-Si_3N_4 is determined solely by the composition of the grain boundary phase,[22] this observation is supported by the XRD-results.

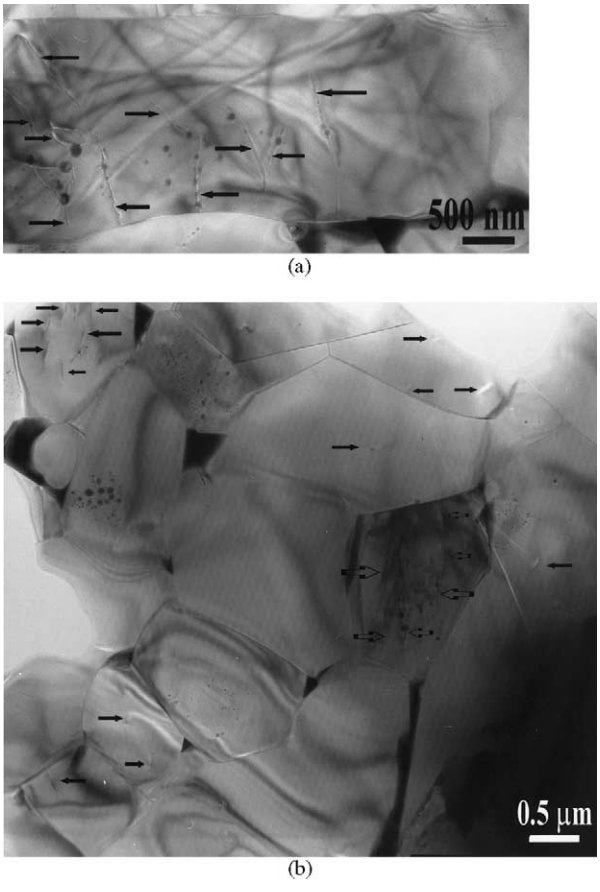

Fig. 3. (a) More detailed BF TEM image of sample A showing β-Si_3N_4 grain containing many second-phase precipitates and mismatch dislocations (marked by black arrows); (b) more detailed BF TEM image of sample A showing about 50% of β-Si_3N_4 grains containing some defects such as precipitates, mismatch dislocations (marked by white arrows), and dislocations without precipitates (marked by black arrows).

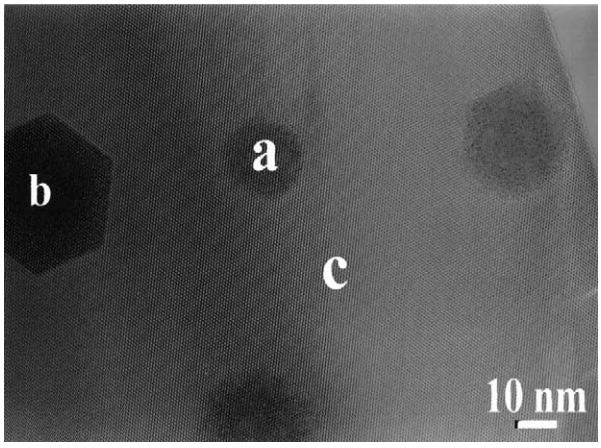

Fig. 4. An enlargement of BF TEM image of sample A of precipitates of the β-Si_3N_4 grain. (a) A round precipitate; (b) a hexagonal precipitate; (c) a matrix.

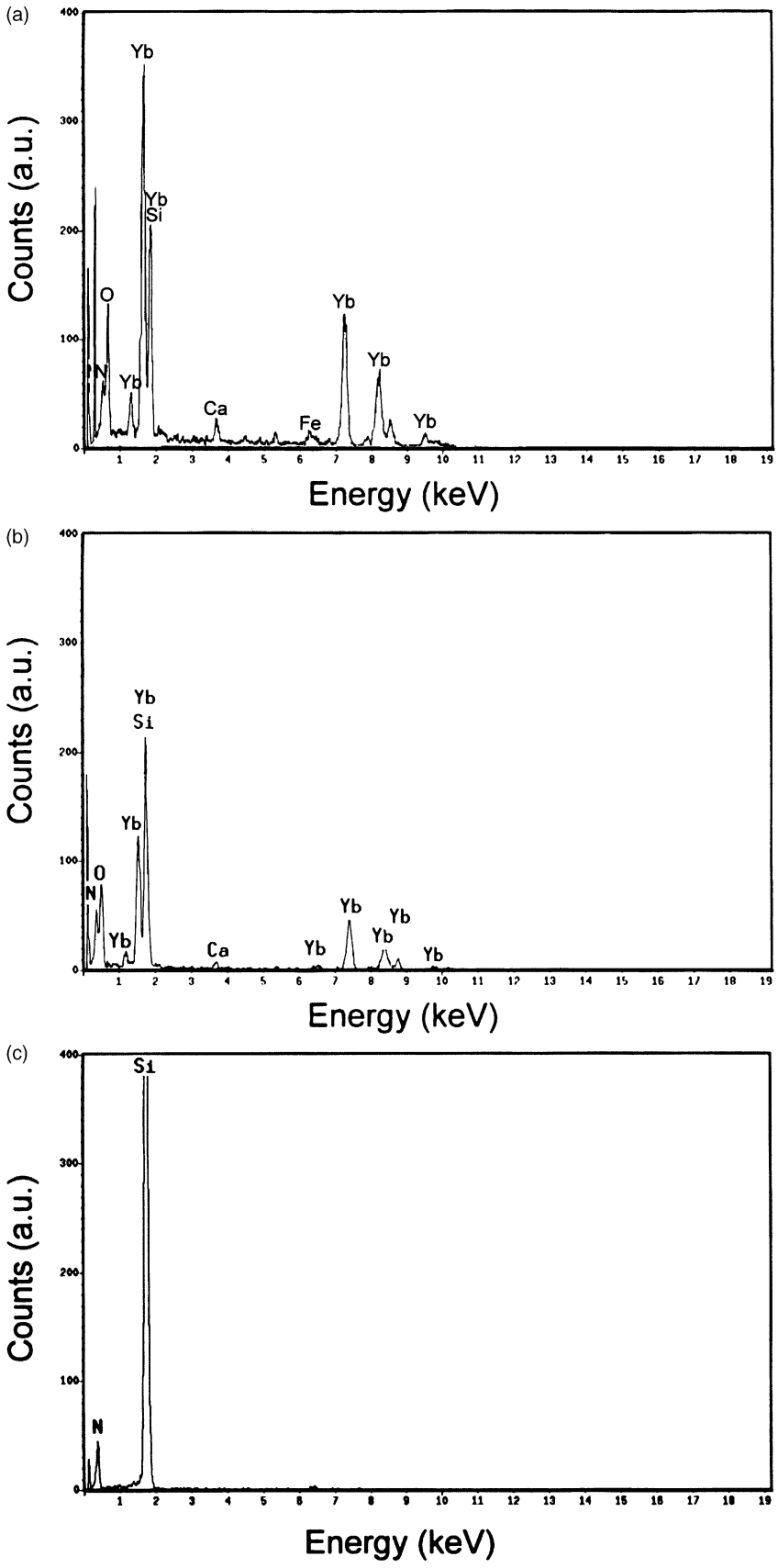

Fig. 5. EDS spectra of sample A obtained from (a) the round precipitate; (b) the hexagonal precipitate; (c) the matrix β-Si_3N_4 grain.

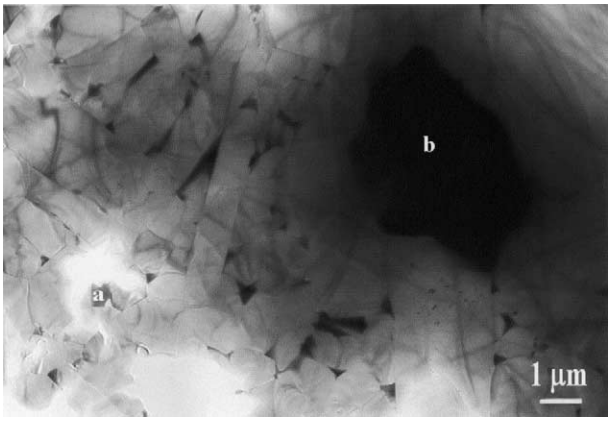

Fig. 6. BF TEM image of sample A.

4. Discussion

In the present work, sintered Si_3N_4 materials with Yb_2O_3 and ZrO_2 as sintering additives were produced to clarify the effect of internal structure on thermal conductivity at room temperature. The longer sintering time and the additional heat treatment significantly promoted grain growth of β-Si_3N_4. It is obvious that these two factors also improved the thermal conductivity, from 110 to 150 $Wm^{-1}K^{-1}$. It should be noted that these two factors also led to a decrease of the lattice defects in the β-Si_3N_4 grains, such as Yb-precipitates, mismatch dislocations which originate from the precipitates, and the grown-in dislocations.

With regard to the grain boundaries, there are no significant differences in the film thickness and the chemical composition of the grain boundary phases between the two specimens. Kitayama et al.[20] revealed that when grain size was $\geqslant 1$ μm, the difference in thermal conductivities was weakly influenced by the glassy phase. In this series of experiments, since the mean grain sizes of the sintered materials were significantly above 1 μm, the observed difference in thermal conductivities was hardly influenced by the grain boundaries.

Hence it follows that the improvement in thermal conductivity of the β-Si_3N_4 is mainly attributable to the improvement of perfection in the β-Si_3N_4 crystal lattice.

As the perfection of the crystal lattice is strongly influenced by precipitates in the β-Si_3N_4 grains, it is important to elucidate the trapping and removing mechanisms of theYb-precipitates to improve the thermal conductivity of sintered Si_3N_4.

The following discussion will first address the possible position of the Yb in the lattice of the β-Si_3N_4 and then will elucidate the mechanisms that are involved in trapping and removing the Yb ion in the β-Si_3N_4. Finally we will discuss the effect of the internal structure on the thermal conductivity.

Rare earth elements do not usually form solid solutions with β-Si_3N_4, but recently, Wang et al. reported that the lanthanide ions (La, Nd, Gd, Yb) were localized inside the with β-Si_3N_4 grains.[23] Since there were no obvious mismatch dislocations in the adjacent trapped regions, they proposed that the trapped lanthanide ions were positioned in the "channel " of the β-SiAlON lattice. [23] Hirosaki et al.[24,25] reported that Y-Nd-Si-O-N of secondary phase particles were trapped and remained in the β-Si_3N_4 grains which were sintered for 8 h at 1900 °C and annealed for 4 h at 2200 °C. Lu et al.[16] also reported that amorphous precipitates were observed at the interface between the core and shell. In the present work, the presence of mismatch dislocations in adjacent regions of the precipitates suggests that the plausible position of Yb in the β-Si_3N_4 lattice is considered to be similar to the case of Al^{3+} and O^{2-} ions replacing Si^{4+} and N^{3-} ions and forming β-SiAlON, the Yb^{3+} and O^{2-} ions replace the Si^{4+} and N^{3-} ions, inducing a substituonal solid solution. However, since some of the precipitates were observed without mismatch dislocations, some of the Yb^{3+} might be positioned in the "channel " of the β- Si_3N_4 lattice as the interstitials.

Secondly we will address the trapping and removing mechanisms. Wang et al. explained the trapping mechanism of rare earth elements into the β-Si_3N_4 grains by using two parameters: the grain-growth speed, V_g, and the migration speed of the R ion (In the present work, $R = Yb^{3+}$), V_p. If $V_p \geqslant V_g$, the R ion will not be trapped; if $V_p < V_g$, the R ion shall likely be trapped in the lattice.[23] Now we can expand their theory for the trapping and removing processes of the Yb-contained liquid phase in the present work. Since we used the raw powder, which contained 48.5 mass% α-phase Si_3N_4, α–β transformation will occur in half of the raw powder at the initial stage of the sintering. Therefore, there are typically two cases to be considered at the initial stage of the sintering in the present work.

4.1. β-nuclei are surrounded only by α-Si_3N_4 grains

When α–β transformation occurs, the relation of $V_p < V_g$ will be expected. It is therefore thought that a portion of Yb included liquid phase was probably trapped by rapid growth during the initial stage of α–β transformation and remained so after homogenization. Although Lu et al.[16] reported that amorphous precipitates were localized at the interface between the core and shell, the precipitates of the present work existed everywhere inside the grains. This is because the longer sintering than that of the experiments of Lu et al.[16] led to the diffusion of the precipitates due to Ostwald ripening.

4.2. β-nuclei are surrounded by only β-Si_3N_4 grains

Grain growth after α–β transformation continues in accordance with Ostwald ripening. The grain growth

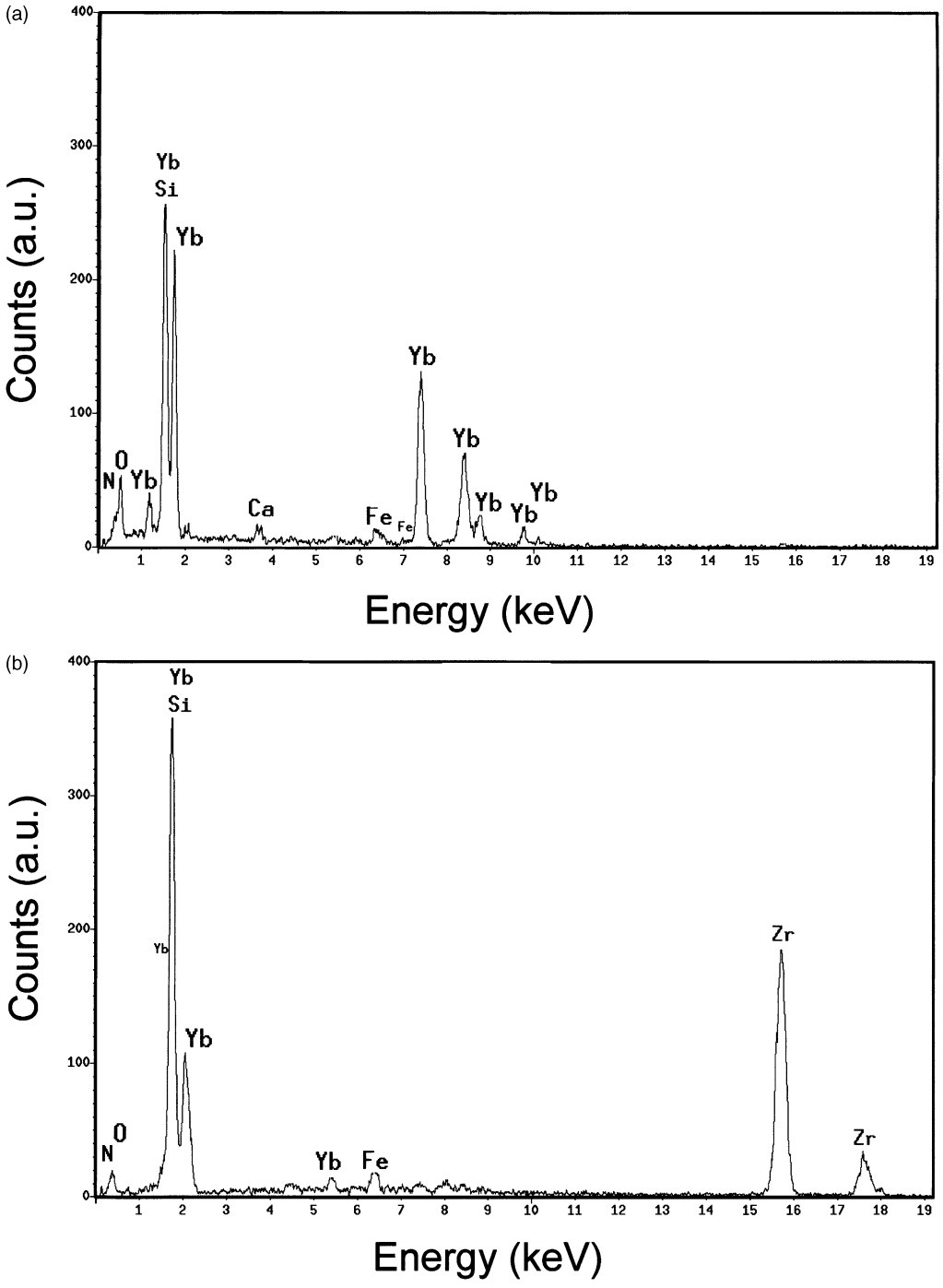

Fig. 7. EDS spectra of the grain boundary phases of (a) a small grain boundary pocket; (b) a large grain boundary pocket.

rate is dependent on the deviation of the grain diameter and the sintering temperature. If grain growth occurs under the $V_p \geqslant V_g$ condition, removal of the trapped precipitates will be expected. The fact of the absence of precipitates in β-Si_3N_4 grains of both 110 $Wm^{-1}K^{-1}$ specimen $\geqslant 2$ μm in diameter and 150 $Wm^{-1}K^{-1}$ specimen suggests that the trapped precipitates are removed as the grain grows. This result reveals that grain growth at between 1700 (annealing temperature at 150 $Wm^{-1}K^{-1}$ specimen) and 1900 °C in the present work would occur under the $V_p \geqslant V_g$ condition. The mismatch dislocations would disappear with the removal of the Yb-precipitates as the grain grows. On the contrary, the Yb containing liquid phase will be trapped under the $V_g \geqslant V_p$ condition (i.e. at very high temperature sintering or annealing), because the mass transport is accelerated with rapid grain growth under the high temperature, the Si_3N_4 grains are completely surrounded by the liquid phase composed of SiO_2 and sintering additives during liquid phase sintering, so rare

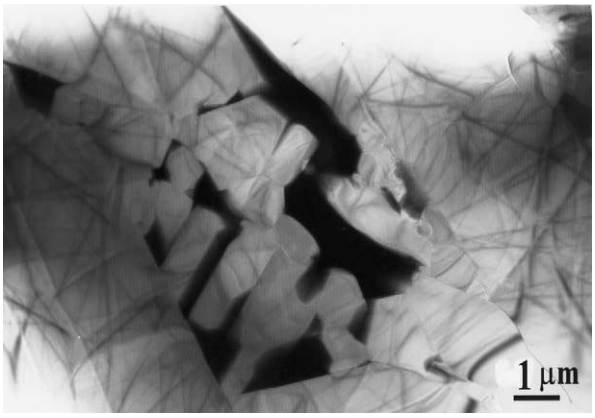

Fig. 8. BF TEM image of the general microstructure of sample B contained without lattice defects, such as precipitates, mismatch dislocations, and grown in of dislocations.

earth elements can be contained in β-Si_3N_4 grains. Indeed, Munakata et al.[15,17] reported that the trapped Y–Nd–Si–O–N of secondary phase particles was grown during the annealing at 2200 °C, even if raw β-Si_3N_4 grains were used.

The reason that the Zr^{4+} contained precipitates could not be observed in the β- Si_3N_4 lattice is not clear at this time. One possible reason is considered that Zr^{4+} cannot form a solid solution with β-Si_3N_4. Another possibility is that the diffusion speed of Zr^{4+} is much faster than that of Yb^{3+}. The fact that the Zr-containing grain boundary phase tends to agglomerate suggests that the Zr-containing liquid phase hardly wets Si_3N_4. Therefore, the former reason is plausible in the present work.

Finally we will discuss the effect of the internal structure on the thermal conductivity. The measured lattice oxygen contents[8–12] were within hundreds of ppm resulting in the range of 10^{17}–10^{19} defects/cm^3 and yield substitutional solute ions, as well as the associated charge compensating defects, in virtually every unit cell, thereby limiting the phonon mean free path to unit cell dimensions. It is therefore likely that the nearly 50% increase in thermal conductivity is not only due to a reduction of the lattice oxygen concentration but also something factor contributing.

As noted earlier, small amounts of rare earth elements tend to form substitutional or interstitial solid solutions with β-Si_3N_4. It should be noted that a solid solution can be substitutional or interstitial of sintering additives affect the thermal conductivity of the β-Si_3N_4, even if the amount of trapped elements is relative low.[24] Attention should also be paid to the point defects and associated mismatch and grown-in dislocations. They scatter the phonons which transport heat, resulting in lower thermal conductivity. With regard to the grown-in dislocations, Lee et al.[13] reported that such dislocations could be reduced by the prolonged annealing. The absence of grown- in dislocations of 150 $Wm^{-1}K^{-1}$ specimen suggests the dislocations disappear as the grain grows. The finding that the chemical compositions of the grain boundary phases are identical for both specimens supports that a volume change did not occur during the prolonged sintering and subsequent annealing.

The grain growth by solution-reprecipitation presumably yields new grains with significantly lower defect concentrations. It is possible that a lower concentration of defects such as precipitates, and dislocations also play a role in the refined and presumable recovered microstructures. The nearly 50% increase in thermal conductivity is therefore due to not only a reduction of the lattice oxygen concentration but also decreasing the lattice defects contributing.

5. Conclusions

Two types of high thermal conductive β-Si_3N_4 ceramics, with 110 $Wm^{-1}K^{-1}$ (8 h sintering at 1900 °C) and 150 $Wm^{-1}K^{-1}$ (36 h sintering at 1900 °C and 100 h annealing at 1700 °C), fabricated by pressureless sintering with Yb_2O_3 and ZrO_2 were investigated by SEM and TEM. The following conclusions can be drawn from the present work.

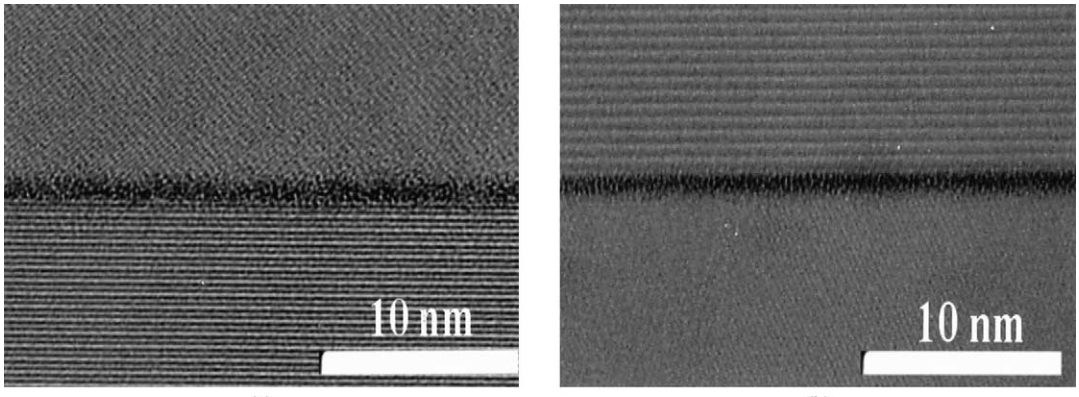

Fig. 9. TEM micrograph of small regions of the grain boundaries of (a) sample A; (b) sample B.

1. The long sintering time and the additional heat treatment significantly promote grain growth of β-Si_3N_4.
2. The prolonged sintering time and the additional heat treatment improve the thermal conductivity, from 110 to 150 $Wm^{-1}K^{-1}$.
3. The prolonged sintering time and the additional heat treatment decrease the lattice defects in the β-Si_3N_4 grains, such as Yb-precipitates, mismatch dislocations and grown-in dislocations.
4. With regard to the grain boundaries, there are no significant differences in the film thickness and the chemical composition of the grain boundary phases between both specimens.

The nearly 50% increase in thermal conductivity of the β-Si_3N_4 is therefore attributed to the reduction of internal defects of the β-Si_3N_4 grains with sintering and annealing time as the grains grow.

References

1. Kingery, W. D., The thermal conductivity of ceramic dielectrics. In *Progress in Ceramic Science, Vol.2*, ed. J. E. Burke. Pergamon Press, New York, 1962, pp. 182–235.
2. Hirosaki, N., Okamoto, Y., Ando, M., Munakata, F. and Akiume, Y., Effect of grain growth on the thermal conductivity of silicon nitride. *J. Ceram. Soc. Jpn*, 1996, **104**(1), 49–53.
3. Hirao, K., Watari, K., Brito, M. E., Toriyama, M. and Kanzaki, S., High thermal conductivity in silicon nitride with anisotropic microstructure. *J. Am. Ceram. Soc.*, 1996, **79**(9), 2485–2488.
4. Watari, K., Hirao, K., Brito, M. E., Toriyama, M. and Kanzaki, S., Hot isostatic pressing to increase thermal conductivity of silicon nitride ceramics. *J. Mater. Res.*, 1999, **14**(4), 1538–1541.
5. Akiume, Y., Munakata, F., Matsuo, K., Okamoto, Y., Hirosaki, N. and Satoh, C., Effect of grain size and grains structure on the thermal conductivity of β-Si_3N_4. *J. Ceram. Soc. Jpn*, 2000, **83**(8), 1985–1992.
6. Watari, K., Hirao, K., Brito, M. E., Toriyama, M. and Ishizaki, K., Effect of grain size on the thermal conductivity of silicon nitride. *J. Am. Ceram. Soc.*, 1999, **82**(3), 777–779.
7. Hirosaki, N., Okamoto, Y., Ando, M., Munakata, F. and Akiume, Y., Thermal conductivity of gas-pressure-sintered silicon nitride. *J. Am. Ceram. Soc.*, 1996, **79**(11), 2878–2882.
8. Kitayama, M., Hirao, K., Tsuge, A., Watari, K., Toriyama, M. and Kanzaki, S., Thermal conductivity of β-Si_3N_4. Part II, effect of lattice oxygen. *J. Am. Ceram. Soc.*, 2000, **83**(8), 1985–1992.
9. Hayashi, H., Hirao, K., Toriyama, M. and Kanzaki, S., $MgSiN_2$ addition as a means of increasing the thermal conductivity of β-silicon nitride. *J. Am. Ceram. Soc.*, 2000, **84**(12), 3060–3062.
10. Hayashi, H., Hirao, K., Kitayama, M., Yamamazaki, Y. and Kanzaki, S., Effect of oxygen content on thermal conductivity of sintered silicon nitride. *J. Ceram. Soc. Jpn*, 2001, **109**(12), 1046–1050.
11. Yokota, H. and Ibukiyama, M., High-thermal conductivity of β-Si_3N_4 prepared by gas pressure sintering. In *Ceramic Transactions, Vol 112, Ceramic Processing Science IV, 7th International Ceramic Processing Science Meeting 2000*, ed. S. Hirano, G. L. Messing and N. Claussen. American Ceramic Society, Westerville, OH, 2001, pp. 611–616.
12. Yokota, H. and Ibukiyama, M., Effect of lattice impurities on the thermal conductivity of β-Si_3N_4. *J. Eur. Ceram. Soc.*, 2003, **23**(1), 55–60.
13. Lee, W. E. and Hilans, G. E., Microstructural changes in β-silicon nitride grains upon crystallizing the grain-boundary glass. *J. Am. Ceram. Soc.*, 1989, **72**(10), 1931–1937.
14. Wang, C. M., Pan, X., Rühle, M., Riley, F. L. and Mitomo, M., Review silicon nitride crystal structure and observations of lattice defects. *J. Mater. Sci.*, 1996, **31**, 5281–5298.
15. Munakata, F., Sato, C., Hirosaki, N., Tanimura, M., Akiume, Y., Okamoto, Y. and Inoue, Y., Annealing effects for structural defects of silicon nitride ceramics. *J. Ceram. Soc. Jpn*, 1997, **105**(10), 5281–5298.
16. Lu, H. H. and Huang, J. L., Microstructure in silicon nitride containing β-phase seeding: III, grain growth and coalescence. *J. Am. Ceram. Soc.*, 2001, **84**(8), 1891–1895.
17. Munakata, F., Sato, C., Hirosaki, N., Tanimura, M., Akiume, Y. and Inoue, Y., TEM observation of microstructure in silicon nitride ceramics containing Y_2O_3–Nd_2O_3 additive. *J. Ceram. Soc. Jpn*, 1998, **106**(4), 441–443.
18. Yokota H., Yamada S., and Ibukiyama M. Effect of amount of β-Si_3N_4 particles on thermal conductivity of β-Si_3N_4 ceramics. *J. Eur. Ceram. Soc.* (in press).
19. Yokota H, and Ibukiyama M., Effect of the addition of β-Si_3N_4 nuclei on the thermal conductivity of β-Si_3N_4 ceramics. *J. Eur. Ceram. Soc.* (in press).
20. Kitayama, M., Hirao, K., Toriyama, M. and Kanzaki, S., Thermal conductivity of β-Si_3N_4. Part I, effects of various microstructural factors. *J. Am. Ceram. Soc.*, 1999, **82**(11), 3105–3112.
21. Kitayama, M., Hirao, K., Watari, K., Toriyama, M. and Kanzaki, S., Thermal conductivity of β-Si_3N_4: III, effect of rare-earth (RE = La, Nd, Gd, Y, Yb, and Sc) oxide additives. *J. Am. Ceram. Soc.*, 2001, **84**(2), 353–358.
22. Kleebe, H. J., Cinibulk, M. K., Cannon, R. M. and Rühle, M., Statistical analysis of the intergranular film thickness in silicon nitride ceramics. *J. Am. Ceram. Soc.*, 1993, **76**(8), 1969–1977.
23. Wang, C. M., Pan, X., Gu, H., Duscher, G., Hoffmann, M. J., Cannon, R. M. and Rühle, M., Transient growth bands in silicon nitride cooled in rare-earth-based glass. *J. Am. Ceram. Soc.*, 1997, **80**(6), 1397–1404.
24. Hirosaki, N., Saito, T., Munakata, F., Tanimura, M., Akiume, Y. and Ikuhara, Y., *J. Mater. Res.*, 1999, **14**(7), 2959–2965.
25. Cao, J. W., Okada, A. and Hirosaki, N., Creep and stress-rupture behavior of Y_2O_3–Nd_2O_3 doped silicon nitrides with different additive contents. *J. Eur. Ceram. Soc.*, 2002, **22**, 237–245.